Three-Dimensional Structure of Gln^{25}-Ribonuclease T_1 at 1.84-Å Resolution: Structural Variations at the Base Recognition and Catalytic Sites[†,‡]

Raghuvir K. Arni,[*,§] Gour P. Pal,[§] K. G. Ravichandran,[∥,⊥] Alexander Tulinsky,[∥] Frederick G. Walz, Jr.,[#] and Peter Metcalf[§]

European Molecular Biology Laboratory, Meyerhofstrasse 1, Postfach 10.2209, D6900 Heidelberg, Germany, Department of Chemistry, Michigan State University, East Lansing, Michigan 48824, and Department of Chemistry, Kent State University, Kent, Ohio 44242

Received August 13, 1991

ABSTRACT: The structure of the Gln^{25} variant of ribonuclease T_1 (RNase T_1) crystallized at pH 7 and at high ionic strength has been solved by molecular replacement using the coordinates of the Lys^{25}-RNase T_1/2′-guanylic acid (2′GMP) complex at pH 5 [Arni et al. (1988) *J. Biol. Chem. 263*, 15358–15368] and refined by energy minimization and stereochemically restrained least-squares minimization to a crystallographic *R*-factor of 14.4% at 1.84-Å resolution. The asymmetric unit contains three molecules, and the final model consists of 2302 protein atoms, 3 sulfates (at the catalytic sites), and 179 solvent water molecules. The estimated root mean square (rms) error in the coordinates is 0.15 Å, and the rms deviation from ideality is 0.018 Å for bond lengths and 1.8° for bond angles. Significant differences are observed between the three molecules in the asymmetric unit at the base recognition and catalytic sites.

Ribonuclease T_1 (RNase T_1;[1] EC 3.1.27.3) is an extracellular enzyme from *Aspergillus oryzae* that cleaves RNA by catalytic transesterification of 3′,5′ diester links to 2′,3′ cyclic diesters at guanylyl residues followed by their catalytic hydrolysis to corresponding 3′ monoesters (Takahashi & Moore, 1982; Heinemann & Hahn, 1989). The catalytic specificity of this endonuclease for guanylyl groups is about a millionfold greater than for adenylyl residues, whereas catalysis at pyrimidine-containing residues has not been observed (Walz et al., 1979). Furthermore, specific enzyme subsites for nucleoside residues at both the 5′ and the 3′ sides of a cleavable guanylyl residue in RNA substrates have been evidenced (Osterman & Walz, 1979). This extensive and specific nucleoside recognition is remarkable considering that RNase T_1 is one of the smallest known enzymes with only 104 amino acid residues. Considering the polyanionic character of its RNA substrate, it is also interesting that RNase T_1 is an acidic protein which carries a net charge of approximately −7 at pH 7 (Iida & Ooi, 1969).

Original studies (Sato & Egami, 1957) and most subsequent work with RNase T_1 used preparations isolated from Taka-Diastase powder (Sankyo Co., Ltd., Tokyo), and the amino acid sequence of this version of the enzyme was characterized by Gln at position 25 (Takahashi, 1971, 1985). However, the first crystallographic structure of RNase T_1 was determined for a preparation of the enzyme from a different source (Luitpold Werke, Munich) which was shown to be a variant form containing Lys at position 25 (Heinemann & Saenger, 1982). The basis of this substitution is currently unknown, but it is likely that these two forms of the protein are related as allozymes (i.e., are allelic variants) rather than being the products of distinct genetic loci (i.e., related as isozymes). Comparisons of Gln^{25}-RNase T_1 and Lys^{25}-RNase T_1 have revealed no differences in catalytic activity; however, the folded structure of the Lys^{25} variant is more stable than the original form by 0.9 kcal/mol under standard conditions (Shirley et al., 1989), which may be due to a salt bridge between Lys25 and Glu28 side chains (Kiefhaber et al., 1990b).

Recent investigations of RNase T_1 have included kinetic (Pace & Creighton, 1986; Kiefhaber et al., 1990a) and thermodynamic (Walz & Kitareewan, 1990; McNutt et al., 1990; Kiefhaber et al., 1990b) studies of protein folding, NMR to elucidate protein structure (Hoffmann & Ruterjans, 1988) and protein–ligand interactions (Schimada & Inagaki, 1990), protein molecular dynamic simulations (MacKerell et al., 1988; Axelsen & Prendergast, 1989), and the application of site-directed mutagenesis to study substrate recognition (Steyaert et al., 1990) and catalysis (Steyaert et al., 1991) or to engineer more stable forms of the enzyme (Nishikawa et al., 1987). Most of this recent work was stimulated by (or required) knowledge of the three-dimensional structure of the enzyme which was first reported for Lys^{25}-RNase T_1 complexed with 2′GMP (Heinemann & Saenger, 1982).

RNase T_1 is now recognized as a member of an extensive gene family of orthologous enzymes from fungi and bacteria that not only evidence sequence similarities (Takahashi, 1985) but also are characterized by similar three-dimensional structures, particularly at their active sites (Hill et al., 1983; Heinemann & Hahn, 1989). At this time, four crystallographic structures of RNase T_1 have been reported in detail, and these include Lys^{25}-RNase T_1 in complexes with 2′GMP (Arni et al., 1987, 1988), G2′5′pG (Koepke et al., 1989), and $H_2VO_4^-$ (Kostrewa et al., 1989) and the Gln^{25} variant complexed with 2′GMP (Sugio et al., 1988). Preliminary crystallographic studies have been reported for Gln^{25}-RNase T_1 or artificial mutants thereof in complexes with a variety of ribonucleotide ligands and oligonucleotide substrate analogues

[†] Supported by a research grant (QF18) from the Deutscher Akademischer Austauschdienst (FRG) to R.K.A.

[‡] Crystallographic coordinates have been deposited with the Brookhaven Protein Data Bank.

[§] European Molecular Biology Laboratory.

[∥] Michigan State University.

[⊥] Present address: Howard Hughes Medical Institute, Dallas, TX 75235-9050.

[#] Kent State University.

[1] Abbreviations: RNase, ribonuclease; 2′GMP, 2′-guanylic acid; G2′5′pG, guanylyl-(2′–5′)-guanylic acid.

0006-2960/92/0431-3126$03.00/0

(Hakoshima et al., 1990a,b). All crystals in the studies cited above were prepared under similar conditions, which employed 10 mM sodium acetate/acetic acid, pH 4.5, 2.5 mM calcium, and 2-methyl-2,4-pentanediol as a precipitating agent. The resulting crystals all belong to the same space group with similar cell constants and a single molecule in the asymmetric unit. In all cases the crystallization was carried out in the presence of a guanine-containing ligand. Considering this uniformity, we have utilized crystals of RNase T_1 grown at pH 7 and high ionic strength in the absence of a guanine-containing ligand (Martin et al., 1980). This has led to the evaluation of the effects of crystal packing and the resulting alternative intermolecular hydrogen bonding pattern on the conformation of the protein. Additionally, the structural information obtained at different pH values and ionic strengths is crucial since electrostatic interactions and their alteration by proton/cation binding appear to be dominating factors that influence conformational stability of folded RNase T_1 (Pace & Grimsley, 1988; Walz & Kitareewan, 1990; McNutt et al., 1990). Since the Gln[25]-RNase T_1 has been the focus of most biophysical and biochemical studies (Takahashi & Moore, 1982), additional structural information for this variant is important in establishing more rigorous structure/function correlations. Lastly, the three molecules that comprise the asymmetric unit are compared here with each other as well as with structures of RNase T_1 complexed with $H_2VO_4^-$ and guanine nucleotides.

Materials and Methods

Crystallization. Gln[25]-RNase T_1 was isolated and purified from Taka-Diastase (a commercial enzyme extract of the culture medium of *A. oryzae*, Sankyo Co., Tokyo) as previously described (Walz & Hoovermann, 1973). In this study, RNase T_1 was crystallized in 55% $(NH_4)_2SO_4$ and 0.1 M potassium phosphate, pH 7 at 20 °C, following the published procedure of Martin et al. (1980), except that micro seeding and vapor diffusion were used instead of macro seeding and batch methods. The crystals obtained at 20 °C were stabilized by cooling to 10 °C during data collection. The crystals belong to the space group $P2_12_12_1$ with a = 91.71 Å, b = 37.54 Å, and c = 77.67 Å and a partial cell volume of 0.69 cm^3/g. The partial cell volume is consistent with the asymmetric unit containing either two or three molecules with 55% or 32% solvent, respectively.

Data Collection. X-ray diffraction data were collected to 1.84-Å resolution from a single crystal using a Xentronics area detector (Blum et al., 1987). Data were measured in three passes with a scan of 90° in ω, and swing angles (2θ) were set to 25° for the first two scans and to 30° for the third scan. The crystal to detector distance was 14 cm. Exposure times were 90, 120, and 200 s, respectively, for each 0.25° data frame. A total of 53 463 reflections were measured, of which 18 062 were unique. Of the 24 053 independent reflections to 1.84 Å, 18 062 were observed (75.1%). The data were reduced using the program XENGEN (Howard, 1988), and the overall R-merge on intensities for the 18 062 reflections was 4.6%.

Molecular Replacement. The structure of Gln[25]-RNase T_1 was solved using molecular replacement techniques, as implemented in the program package MERLOT (Fitzgerald, 1988). The search model used was the refined structure of Lys[25]-RNase T_1 complexed with 2′GMP (Arni et al., 1987, 1988). For the rotational searches structure factors were calculated in a $P1$ cell with edge dimensions of 70 Å. Data with $I > 3\sigma_I$ between 8.0 and 3.4 Å were used with a radius of integration of 20 Å. The three highest peaks in the cross-rotation map were 7.0σ, 5.3σ, and 4.7σ. The self-rotation and the Crowther fast rotation functions (Crowther, 1972) revealed the orientation of the three molecules in the asymmetric unit. The rotational angles were refined using the Lattman rotation function (Lattman & Love, 1972) with a step size of α = 1°, β = 1°, and γ = 2°.

Structure factors for the translation search were calculated in a $P1$ cell with edge dimensions of 100 Å using data between 8.0 and 3.4 Å. The highest peaks in each section of the Crowther and Blow translation function (Crowther & Blow, 1967) with σ values 5.3 and 4.0 produced a model with reasonable packing. The translational and rotational parameters were further optimized using the R-factor minimization procedure as implemented in the program package MERLOT (Fitzgerald, 1988) which reduced the R-factor from 47.4% for the data with $I > 5\sigma_I$ between 8 and 4.2 Å to 34.5% for data with $I > 3\sigma_I$ in the resolution range 6–2.5 Å.

Refinement. Energy minimization and refinement using XPLOR (Brunger et al., 1987) led to an R-factor of 25.6% for data between 6 and 2.0 Å. After model building, the refinement was continued using a space group specific version of the program PROLSQ (Hendrickson & Konnert, 1980). The structure was refined in nine stages, totaling 87 cycles. At the end of each stage $2F_o - F_c$, $F_o - F_c$, and fragment-deleted maps with coefficients $2F_o - F_c$ (omit maps) were used as an aid in model building which was carried out with FRODO (Jones, 1987) on an Evans and Sutherland PS390 color graphics system.

Solvent molecules were located in the difference maps, and from an early stage in the refinement a large peak was observed close to the site occupied by phosphate in the structure of this enzyme complexed with 2′GMP. Comparison of the difference and double difference maps clearly indicated the presence of a tetrahedrally coordinated site which was subsequently refined as a sulfate ion. Even though sulfate and phosphate cannot be distinguished since they have similar scattering factors, this anion was identified as sulfate since the concentration of sulfate is approximately 20-fold greater than that of phosphate during and after crystallization.

The final model consists of 2302 protein atoms, 3 sulfate ions, and 179 solvent water atoms. A summary of the stereochemical parameters is presented in Table I.

Refinement Results

The present refinement has been concluded after 87 least-squares cycles, with a resulting R-factor of 14.4% for the 16 957 reflections with $I > 1\sigma_I$ in the resolution range 6.0–1.8 Å. The arrangement and identification of the three molecules in the asymmetric unit is illustrated in Figure 1. A total of 28, 10, and 4 protein atoms are poorly defined in the $2F_o$–F_c electron density map for molecules 1, 2, and 3, respectively. These include all of Tyr45 and the side chain of Asn43 in molecule 1 as well as the side chain of Asn98 in molecule 2.

A Luzzati plot (Luzzati, 1952) is illustrated in Figure 2, where the R-factor is expressed as a function of resolution. The plot suggests a mean coordinate error of 0.15 Å. The lowest R values are in the 3.5–4.5-Å range, which also possesses the highest values for the average structure factor amplitudes. Typically, the R values increase at lower resolution presumably due to the omission of hydrogen atoms and the fact that disordered solvent has not been accounted for (Phillips, 1980). At higher resolution the increase in the R-factor can be attributed to the lower accuracy of measurement of the weak, high-resolution reflections.

The main-chain ϕ/ψ torsion angles are clustered in the allowed regions of the Ramachandran plot (Figure 3). Of

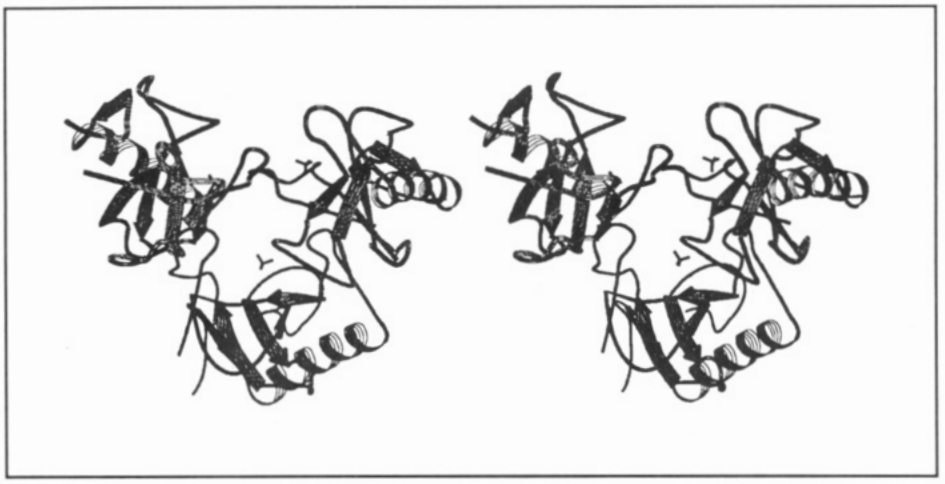

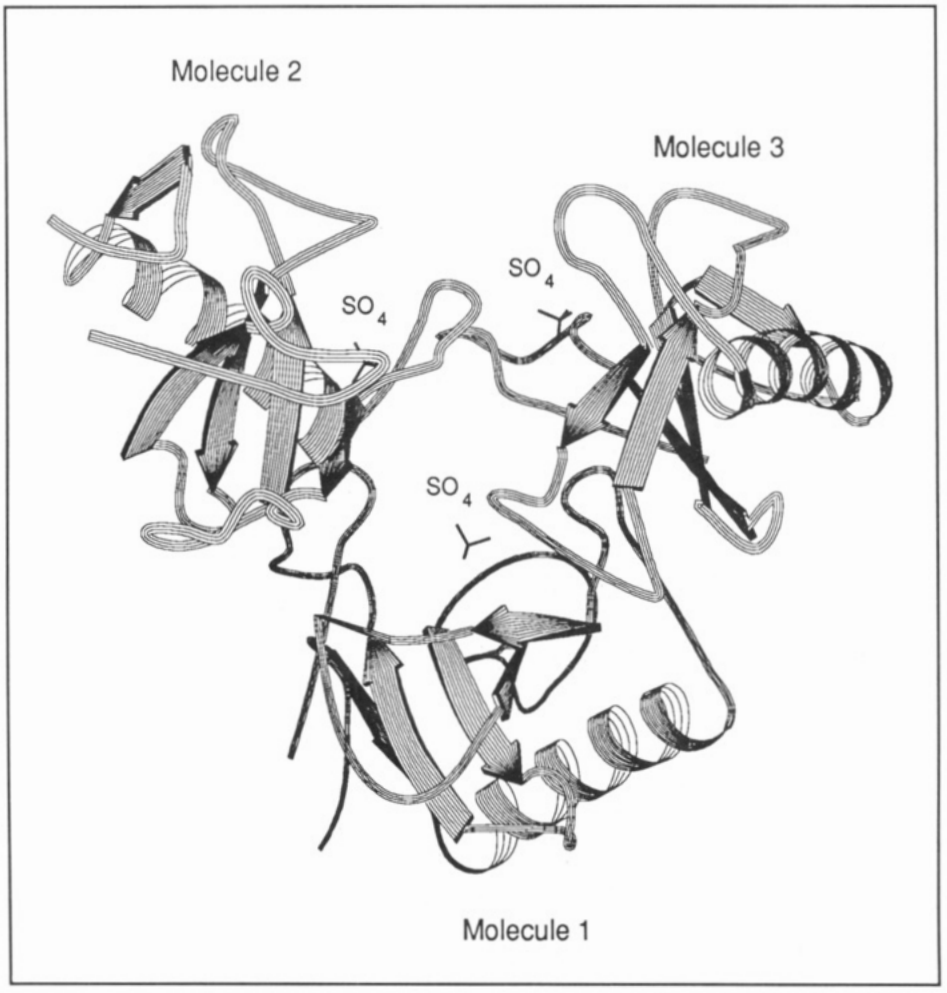

FIGURE 1: View of the three RNase T_1/sulfate molecules in the asymmetric unit. Top: Stereoview. Bottom: Ribbon representation of the three RNase T_1/sulfate molecules. The sulfates are labeled.

the non-glycine residues, amino acids Ser37, Asn44, and Asn84 lie in the region associated with left-handed helices (Ramachandran & Sashisekharan, 1968). In all three molecules Ser37 is involved in tight turns. The ϕ torsion angle of Asn44 in molecule 1 also places it in approximately this region; however, since the electron density for Tyr45 is missing, no assignment for the ψ angle can be made. The torsion angles of Asn44 in molecules 2 and 3 and Asn84 in all three molecules are located in the region assigned to left-handed helices. These three amino acids are involved in tight turns and adopt similar configurations in the structures of RNase T_1 complexed with 2′GMP, G2′5′pG, and vanadate. Ravichandran and Subramaniam (1981) have noted the tendency of asparagine residues to adopt backbone torsion angles that place them in the region of the Ramachandran plot associated with left-handed helices. The single outlier is Asn98 in molecule 3 which is well-defined in the electron density and has ϕ/ψ angles of 69° and 18°, respectively.

The local mobility as represented by the mean crystallographic temperature factors is shown in Figure 4. The regions of high mobility are associated with external loops, whereas the regions of low B value include those residues which are

Table I: Refinement Statistics of the Final Model

Summary	
R-factor (%)	14.4
resolution (Å)	6.0–1.84
no. of reflections	16957
no. of atoms	2496
Root Mean Square Deviations from Ideality (Target Restraints)	
distance restraint information (Å)	
bond distance	0.018 (0.020
angle distance	0.039 (0.030)
planar 1–4 distance	0.057 (0.060)
plane restraint information (Å)	
rms error	0.018 (0.020)
chiral center restraints (Å^3)	
rms error	0.182 (0.150)
nonbonded contact restraints (Å)	
single-torsion contact	0.17 (0.5)
multiple-torsion contact	0.25 (0.5)
possible (X–Y) hydrogen bond	0.19 (0.5)
conformational torsion angles (deg)	
planar	3.3 (5.0)
staggered	14.3 (20.0)
orthonormal	24.2 (25.0)
isotropic temperature factor restraints (Å^2)	
main-chain bond	2.1 (2.0)
main-chain angle	2.9 (3.0)
side-chain bond	5.1 (4.5)
side-chain angle	6.4 (6.0)
av bond angle (deg)	117.3
rms deviation	1.8

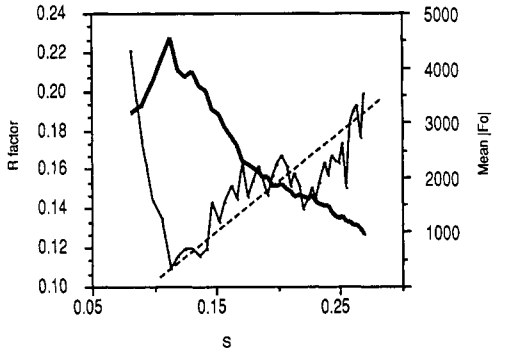

FIGURE 2: Estimation of the mean coordinate error based on the method of Luzzati (1952). The variation of the crystallographic *R*-factor (thin line) and the mean intensities (thick line) expressed as a function of resolution S [$S = (\sin\theta/\lambda)$] are superimposed on the theoretical curve (dashed line) calculated for a mean coordinate error of 0.15 Å.

involved in extensive hydrogen bonding, i.e., the α-helices, β-strands, and intermolecular contacts.

Discussion

RNase T_1 is a compact molecule with a hydrophobic core sandwiched between a 4.5 turn α-helix and a five-stranded antiparallel β-sheet. The polypeptide chain at the amino terminus forms a tight turn, and a disulfide bridge is formed between residues 2 and 10. A second disulfide bridge between residues 6 and 103 links the carboxyl and amino termini of the molecule. The three molecules in the asymmetric unit are shown schematically in Figure 1. The low solvent content of 32% and the presence of three molecules in the asymmetric unit result in a more densely packed structure with many more intermolecular contacts than in the previously determined structures of RNase T_1 in which the asymmetric unit comprises a single molecule with approximately 46% solvent.

The deviations between the corresponding atoms of the three molecules in the asymmetric unit after least-squares alignment of their main-chain atoms are illustrated in Figure 5. The

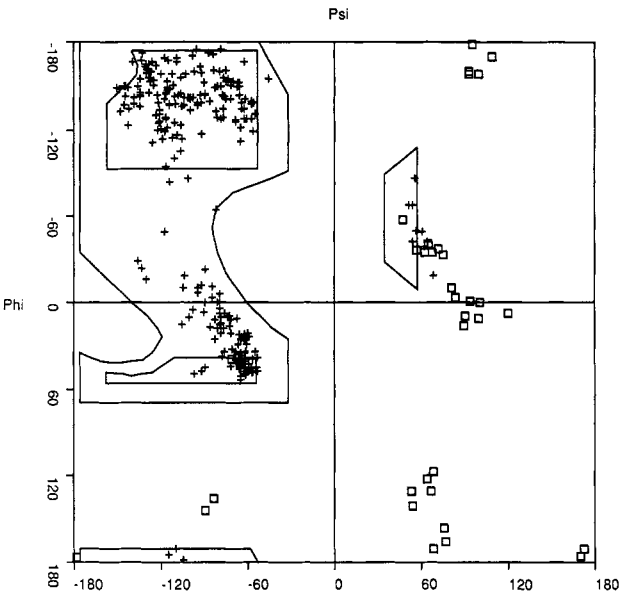

FIGURE 3: Ramachandran plot (Ramachandran & Sashisekharan, 1968). Squares and crosses indicate conformational angles for glycine and non-glycine residues, respectively. The preferred regions are indicated and enclose most non-glycine residues.

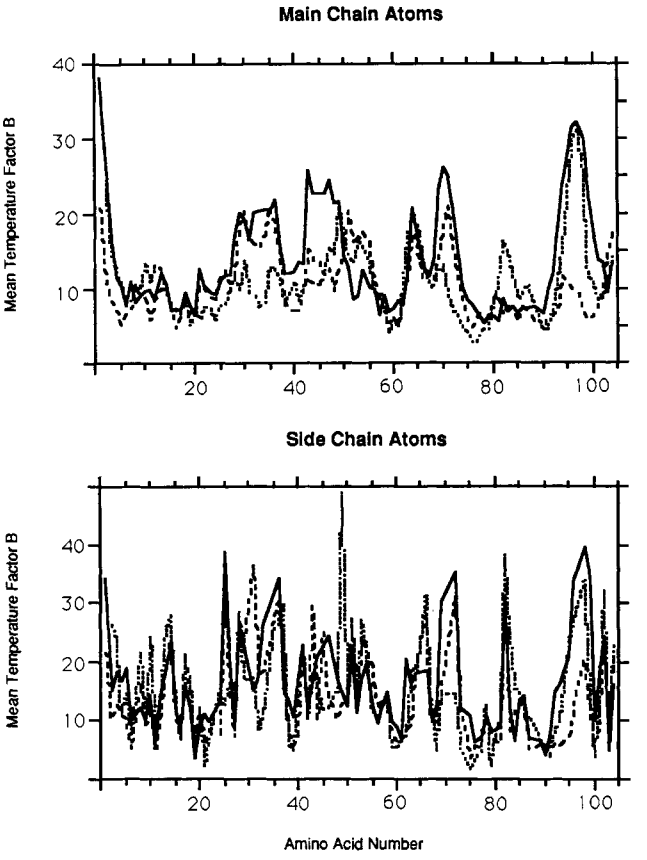

FIGURE 4: Variation of the mean temperature factors, *B*, for the main-chain atoms (upper) and side-chain atoms (lower). Solid, dotted, and dashed lines represent molecules 1, 2, and 3, respectively.

overall rms deviations for the aligned molecules were 0.52 Å for molecules 1 and 2, 0.49 Å for molecules 1 and 3, and 0.48 Å for molecules 2 and 3. Regions of maximum deviation for the main-chain atoms are the carboxy terminus, two surface loops (amino acids 69–72 and 94–99), and the region containing the amino acids involved in base recognition (amino acids 43–46).

Base Recognition Site. The region of the polypeptide chain known to bind with the guanine moiety of 2′GMP consists of

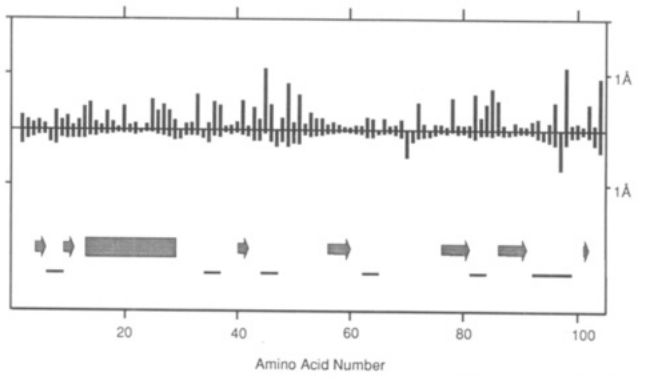

FIGURE 5: Root mean square deviations between the three molecules of the Gln^{25}-RNase T_1/sulfate complex. Values for side-chain and main-chain atoms are presented above and below the line. Shaded arrows, horizontal bars, and the shaded box represent β-strands, turns, and α-helix, respectively.

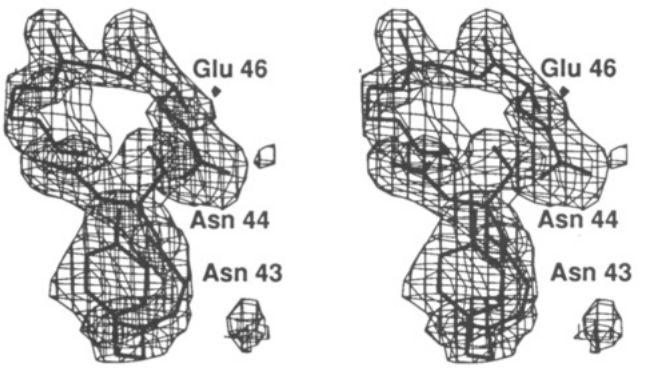

FIGURE 6: Stereoview of the base recognition site of molecule 1 in the final electron density map. Note the absence of density for Tyr45 and the side chain of Asn43.

amino acids 42–46 and 98 (Arni et al., 1988). This site is located in a shallow surface cleft on the outer side of the β sheet and involves part of the large surface loop from residues 42 to 56. Comparison of the local environments of the base recognition regions in the three molecules indicates differences in solvent accessibilities due to crystal packing. The region of the polypeptide chain involved in base recognition in molecule 1 is exposed to the bulk solvent. Most of the atoms in this region are well-defined in the electron density map. However, electron density for the side-chain atoms of Asn43 and for all the atoms of Tyr45 is absent (Figure 6). In molecule 2, the exclusion of solvent from this region by a proximity of a symmetry-equivalent molecule results in reduced flexibility, and all the atoms including the side-chain atoms of Asn43 and Tyr45 are well-defined in the electron density map. Molecule 3 exists in an intermediate stage where the presence of well-ordered solvent contributes to partially reduced flexibility of this region. Most of the atoms are clearly defined in the electron density in this region except for the Tyr45 Oη for which density is absent.

The distribution of temperature factors (Figure 4) gives a further indication of the flexibilities of these regions. Molecule 1 possesses the highest temperature factors and the greatest disorder, followed by molecule 3 and then molecule 2 which is comparatively well-ordered. The temperature factors of residues 42–46 of molecules 2 and 3 are in general comparable with those of the same region of the RNase T_1/2′GMP complex while for this region of molecule 1 they are almost twice as large. This indicates that occupancy of the base recognition site by a guanine group is not the only factor to decrease mobility in this region.[2]

Results of superpositioning the main-chain atoms in the base recognition site (using main-chain atoms of residues 40–46) are illustrated for the three molecules in Figure 7. The hydrogen bonding pattern for this region is shown in Figure 8. In the case of molecules 1 and 3, no solvent molecules are located in this region. In molecule 2, five solvent waters form a network of hydrogen bonds stabilizing the conformation. In all three molecules the carbonyl oxygen of Tyr42 points away from the base recognition site and is hydrogen bonded to a solvent molecule.

It was previously observed that the backbone carbonyl oxygen of Asn98 was hydrogen bonded with N2 of guanine in all complexes of RNase T_1 where this moiety occupied the base recognition site (Arni et al., 1988; Koepke et al., 1989; Lenz et al., 1991). On the other hand, the side chain of Asn98 in various complexes has been shown to hydrogen bond with either Oη of Tyr45 and bound vanadate (Kostrewa et al., 1989) or O5′ of bound guanosine (Lenz et al., 1991), or via water bridges making intermolecular or intramolecular protein contacts in the crystal (Arni et al. 1988; Koepka et al., 1989). The results of the present study indicate even greater diversity for this residue. In molecule 1, both the backbone amide nitrogen and Nδ2 of Asn98 form hydrogen bonds to the backbone carbonyl oxygen of Glu28 from molecule 2 and Nδ2 also forms an intramolecular hydrogen bond with Oδ1 of Asn99. In molecule 2, Asn98 adopts a different conformation. The backbone carbonyl oxygen is now hydrogen bonded with a water bridge to Oϵ1 of Glu46 which is similar to that found in the presence of bound guanine where the exocyclic amino group (N2) of the base assumes the bridge position. The main-chain amide nitrogen is hydrogen bonded to a water molecule, but the side chain of Asn98 in molecule 2 is disordered. In molecule 3, the backbone atoms of this residue have a similar conformation as molecule 2, but the amide nitrogen is now hydrogen bonded to Oϵ1 of Gln85 from a symmetry-related molecule in addition to a solvent molecule. The side chain forms hydrogen bonds with the bound sulfate as well as with a water and Oδ1 of Asn83 from a symmetry-related molecule. The sum of these observations regarding Asn98 emphasizes the dramatic effects that different crystal environments and different bound ligands can have on the conformation, dynamics, and hydrogen bonding patterns for a given polar residue on the surface of a protein.

The main-chain atoms of the base recognition sites of molecule 2 of Gln^{25}-RNase T_1/sulfate, Lys^{25}-RNase T_1/2′GMP, and Lys^{25}-RNase T_1/vanadate are shown superposed in Figure 9. Significant differences occur between the sulfate and vanadate complexes even though both lack a guanine base group. The flipped peptide bond between Asn43 and Asn44 which was observed in the vanadate complex (Kostrewa et al. 1989) was not observed in any of the three molecules in this study.

The Catalytic Site. In the structure of the Lys^{25}-RNase T_1/2′GMP complex (Arni et al., 1987, 1988), the sugar–phosphate of the bound inhibitor protrudes into a shallow depression and the phosphate group interacts with the side chains of Tyr38, His40, Glu58, Arg77, and His92. In the present structure, density corresponding to tetrahedrally coordinated ions is present in similar positions as the phosphate group of 2′GMP and is interpreted as representing sulfate ions. In contrast with the base recognition site, relatively small root mean square (rms) deviations characterize backbone and

[2] Preliminary refinement results of these crystals with 8-iodoguanosine bound at pH 5.5 suggest that this ligand occupies the base recognition site, which results in reduced mobility of amino acid residues at this locus.

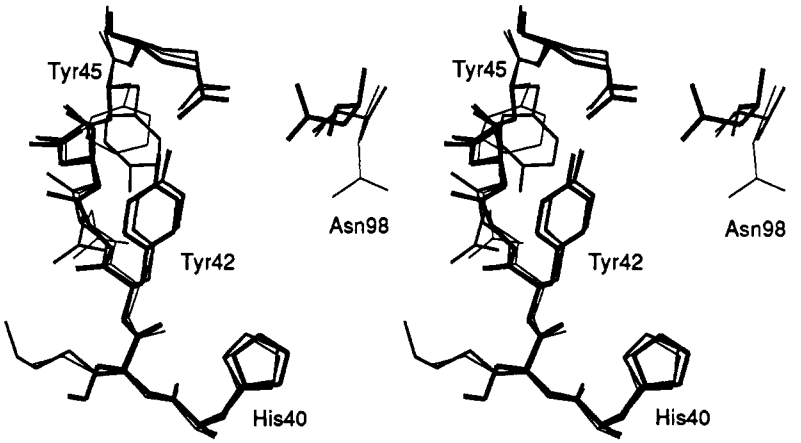

FIGURE 7: Superposed base recognition sites of the three molecules composing the asymmetric unit of Gln[25]-RNase T_1/sulfate. His40 through Glu46 and Asn98 are shown. Thick, medium, and thin lines represent molecules 1, 2, and 3, respectively.

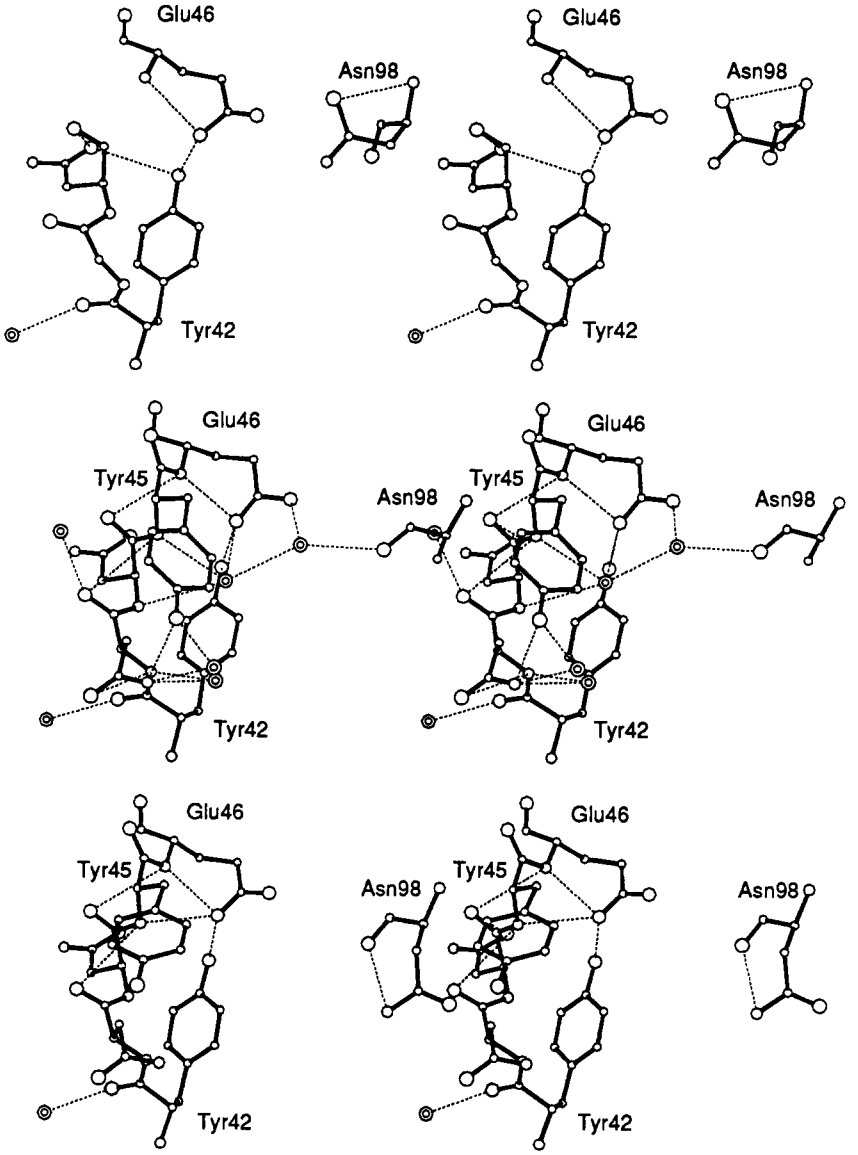

FIGURE 8: Stereoview of hydrogen bonding in the base recognition sites of the Gln[25]-RNaseT_1/sulfate complexes. Atoms representing residues Tyr42 through Glu46 and Asn98 are shown if determined. Solvent molecules are shown as concentric circles. Top, middle, and bottom diagrams represent molecules 1, 2, and 3, respectively.

side-chain atoms of residues at the catalytic site comparing the three molecules in the asymmetric unit (Figure 5) as well as in comparisons involving the structures of Lys[25]-RNase T_1/2′GMP, Lys[25]-RNase T_1/G2′5′pG, and Lys[25]-RNase $T_1/H_2VO_4^-$ (data not shown). Furthermore, the backbone and side-chain atoms of residues composing this site are characterized by temperature factors that are almost always among the lowest reported for RNase T_1 complexes with either sulfate (see Figure 4), 2′GMP (Arni et al., 1988), or $H_2VO_4^-$ (Kostrewa et al., 1989).

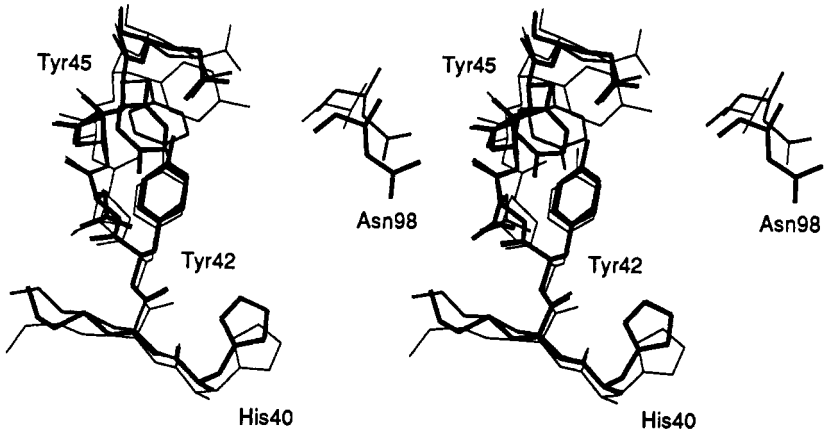

FIGURE 9: Stereoviews of superposed base recognition sites of the Gln^{25}-RNase T_1/sulfate complex (molecule 2) with 2'GMP and vanadate complexes with Lys^{25}-RNase T_1. His40 through Glu46 and Asn98 are shown. Thick, medium, and thin lines represent the sulfate, 2'GMP, and vanadate complexes, respectively.

Table II: Hydrogen Bonds of Tetrahedrally Coordinated Anions at the Active Site of RNase T_1[a]

molecule 1			molecule 2			molecule 3			2'GMP			$H_2VO_4^-$		
O1	NH2 Arg77	2.48	O1	NH2 Arg77	2.55	O1	NH2 Arg77	2.72	O1	O Wat158	2.63	O1	NH2 Arg77	3.16
	Nε Arg77	2.68		Nε Arg77	3.15		Nε Arg77	3.12		O Wat179	3.02		Nε Arg77	2.59
	Nε2 His92	3.22		Nε2 His92	2.59		Nε2 His92	2.62		O Wat186	2.73		Nε2 His92	2.79
	Oε2 Glu58	3.00											Oε2 Glu58	2.94
	OH Tyr38	3.19		OH Tyr38	3.42									
O2	Oε1 Glu58	3.29	O2	Oε1 Glu58	2.88	O2	Oε1 Glu58	3.25	O2	Oε1 Glu58	2.70	O2	Oε1 Glu58	2.68
	Oε2 Glu58	2.74		Oε2 Glu58	2.69		Oε2 Glu58	2.82		Oε2 Glu58	2.38		Oε2 Glu58	3.13
	Nε His40	3.41											O Wat175	2.8
O3	Nε His40	3.08	O3	Nε2 His40	3.28	O3	Nε2 His40	2.94	O3	Nε2 His40	2.84	O3	Nε2 His40	3.00
	OH Tyr38	2.29		OH Tyr38	2.37		OH Tyr38	2.63		Oε2 Glu58	3.40		OH Tyr38	2.58
				Oε2 Glu58	3.39		Oε2 Glu58	3.50		OH Tyr38	2.70		O Wat176	2.59
							O Wat454	2.93						
O4	Nε His92	3.49	O4			O4			O4			O4	Nε2 His92	3.49
							Oδ1 Asn98	3.38					Oδ1 Asn98	3.14
							Nδ2 Asn98	3.09					O Wat266	3.26
							O Wat454	3.32					O Wat183	2.8

[a] The three columns in each group show the anionic oxygen, the bonded atom, and the bond donor–acceptor distance (Å), respectively. The donor–acceptor distance threshold used was 3.5 Å.

Even though the catalytic site appears to be constrained regarding its conformation and dynamics, the pattern of its hydrogen bonding with anions shows considerable variation. In all cases, hydrogen bonds with anions at the catalytic site involve side-chain atoms exclusively, and these are described in Figure 10 and Table II. In molecule 1, eleven hydrogen bonds are formed involving all sulfate oxygens. In molecule 2, nine such bonds are formed but one sulfate oxygen has no fixed hydrogen bonding. In molecule 3 twelve hydrogen bonds can be assigned including two from a water molecule and two from both side-chain atoms (Oδ1 and Nδ2) of Asn98. Molecule 3 and the vanadate complex are the only cases where Asn98 has been shown to participate in hydrogen bonding at the catalytic site, with the anion also being hydrogen bonded with fixed waters. Therefore, it appears that the catalytic site interactions for sulfate in molecule 3 most closely represent those for the vanadate complex. However, the mean temperature factor for sulfate atoms in molecule 3 is 17 $Å^2$, which is considerably less than that for the vanadate anion (Kostrewa et al., 1989). Common features for binding oxygen atoms of either sulfate or vanadate anions are as follows: O1 involves Arg77 (two bonds) and His92, O2 only involves Glu58, O3 involves Tyr38 and His40, and O4 involves weak hydrogen bonds (i.e., with His92 and Asn98) if any are observed at all. The strong hydrogen bonds involving Glu58 and Tyr38 are also observed with phosphate in the 2'GMP complex. The intimacy of the γ-carboxyl group of Glu58 with anionic oxygen atoms is surprising since it might have been supposed that positively charged groups at the catalytic site would dominate interactions with anionic groups. As discussed previously, the carboxyl group of Glu58 assumes a high pK_a value when adjacent to the phosphate group of 2'GMP (Arni et al., 1988). However, it might have been supposed that the free energy for this increased pK_a was made available by tight binding of the guanine moiety of 2'GMP; in view of the present results with sulfate binding it appears that this is not the case.

Conclusion

Structural differences between the three Gln^{25}-RNase T_1/sulfate molecules in the asymmetric unit should only reflect differences in intermolecular interactions resulting from crystal packing, whereas differences between these molecules and complexes of Lys^{25}-RNase T_1 with 2'GMP or vanadate could also result from the residue substitution at position 25 as well as different solvent conditions. At first view it might be surprising that the dramatic differences in pH and ionic strength for the solvents used in the present and previous studies (see above) appear to have little or only small effects on RNase T_1 structure. However, this finding may not be unexpected because electrostatic destabilization of the protein would be attenuated by the lower pH and the amino acid substitution in previous studies with crystals of Lys^{25}-RNase T_1.

It is reasonable to assume that the base recognition site of uncomplexed RNaseT_1 in solution would most closely resemble that found for molecule 1 in crystals of Gln^{25}-RNase T_1/sulfate

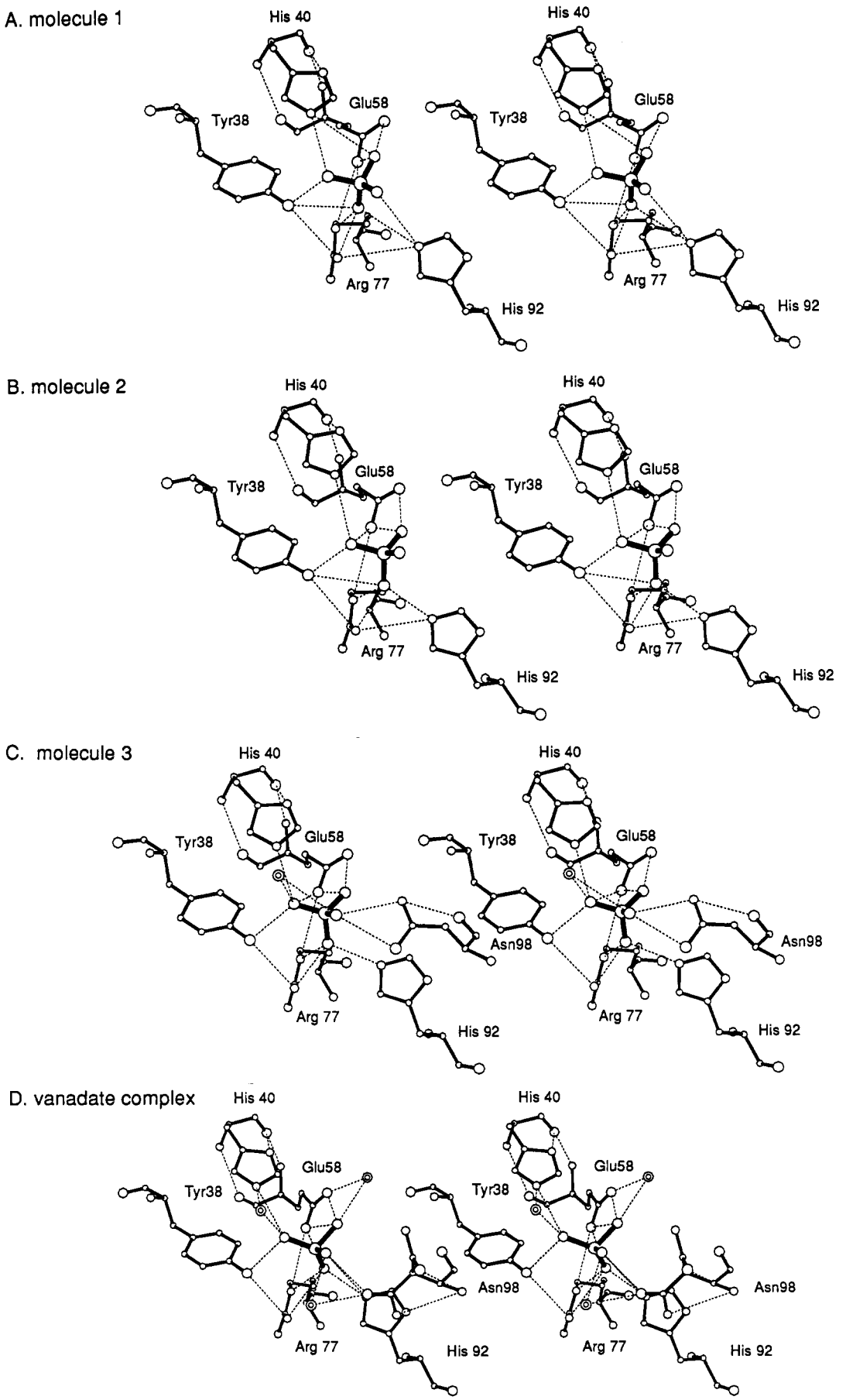

FIGURE 10: Stereoviews of the catalytic sites of the Gln[25]-RNase T_1/sulfate complex and the Lys[25]-RNase T_1/vanadate complexes. Backbone and side-chain atoms of Tyr38, His40, Glu58, Arg77, His92, and Asn98 are shown if any constituent atom is hydrogen bonded to the sulfate. Hydrogen bonding between His40 and Glu58 backbone atoms is also included. Water molecules are shown as concentric circles. (A) Molecule 1 of the sulfate complex; (B) molecule 2 of the sulfate complex; (C) molecule 3 of the sulfate complex; (D) the vanadate complex.

since this site is the most exposed to solvent among the three base recognition sites in the asymmetric unit. Therefore, it is likely that the uncomplexed site is mobile, being characterized by relatively large excursions of side chains for Tyr45 and Asn43. Furthermore, the existence of three considerably different structures for this region in the same crystal indicates the conformational variability of this site and emphasizes the subtle influence of crystal packing interactions on local structures at protein surfaces. The present findings are in contrast with the previous view that the well-defined structure of the base recognition site in the RNase T_1/vanadate complex is representative of the free enzyme (Kostrewa et al., 1989). It is interesting that the latter structure and one deduced for the free enzyme from a molecular dynamics simulation (MacKerrel et al., 1989) have a "flipped" peptide bond between Asn43 and Asn44 which was not observed in this study. It is possible that this conformation is dependent on the presence of a guanine-containing ligand (i.e., the crystals of Lys^{25}-RNase T_1/vanadate were grown in the presence of guanosine and coordinates for the Lys^{25}-RNase T_1/2'GMP were used to initiate the molecular dynamics simulation).

Recent X-ray crystallographic studies on RNase Sa, which is a bacterial orthologue of RNase T_1, indicated that the conformation of the base recognition site is virtually identical in the presence and absence of specifically bound 3'GMP and that guanine binding results, in part, by substituting for hydrogen-bound waters (Sevcik et al., 1991). However, in the RNase Sa/3'GMP complex one side of the guanine ring is exposed to solvent; i.e., there is no residue corresponding to Tyr45 of RNase T_1 whose side chain stacks on this surface of the guanine group in the RNase T_1/2'GMP complex. It would be interesting to contrast the equilibrium and kinetic properties of guanine nucleotide binding with RNase Sa and RNase T_1 (Mackerell et al., 1991) to elucidate the effect of these alternate modes of binding the guanine moiety.

A detailed description of protein–protein interactions in the crystal lattice of Gln^{25}-RNase T_1/sulfate is underway which should clarify the effects of these interactions on the structures at the active site. Likewise, a description of the water molecules in the present structure will be undertaken to test whether the "structural conserved water" described for other crystal forms of RNase T_1 (Malin et al., 1991) are found in a different crystal environment.

ACKNOWLEDGMENTS

We gratefully acknowledge the expert assistance of Dr. P. Tucker (EMBL Heidelberg) with data collection.

Registry No. RNase T_1, 9026-12-4.

REFERENCES

Arni, R., Heinemann, U., Maslowska, M., Tokuoka, R., & Saenger, W. (1987) *Acta Crystallogr., Sect. B 43*, 548–554.

Arni, R., Heinemann, U., Tokuoka, R., & Saenger, W. (1988) *J. Biol. Chem. 263*, 15358–15368.

Axelsen, P. H., & Prendergast, F. G. (1989) *Biophys. J. 56*, 43–66.

Blum, M., Metcalf, P., Harrison, S. C., & Wiley, D. C. (1987) *J. Appl. Crystallogr. 20*, 235–242.

Brunger, A. T., Kuriyan, J., & Karplus, M. (1987) *Science 235*, 458–460.

Crowther, R. A. (1972) in *The Molecular Replacement Method* (Rossmann, M. G., Ed.) pp 173–178, Gordon and Breach, New York.

Crowther, R. A., & Blow, D. M. (1967) *Acta Crystallogr. 23*, 544–548.

Egami, F., & Nakamura, K. (1969) *Mol. Biol., Biochem. Biophys. 6*, 1–80.

Fitzgerald, P. M. D. (1988) *J. Appl. Crystallogr. 21*, 273–278.

Hakoshima, T., Oka, K., Toda, S., Tanaka, M., Goda, K., Higo, T., Itoh, T., Minami, H., Tomita, K., Nishikawa, S., Morioka, H., Imura, J., Usegui, S., Ohtsuka, E., & Ikehara, M. (1990a) *J. Biochem. 108*, 695–698.

Hakoshima, T., Itoh, T., Tomita, K., Nishikawa, S., Morioka, H., Usegui, S., Oka, K., Toda, S., Tanaka, M., Goda, K., Higo, T., Ohtsuka, E., & Ikehara, M. (1990a) *J. Mol. Biol. 216*, 497–499.

Heinemann, U., & Saenger, W. (1982) *Nature (London) 299*, 27–31.

Heinemann, U., & Hahn, U. (1989) in *Protein–Nucleic Acid Interactions* (Saenger, W., & Heinemann, U., Eds.) pp 111–141, CRC Press, Boca Raton, FL.

Hendrickson, W. A., & Konnert, J. H. (1980) in *Computing in Crystallography* (Diamond, R., Ramaseshan, S., & Venkateshan, K., Eds.) 13.01–13.23, Indian Academy of Sciences, Bangalore.

Hill, C., Dodson, G., Heinemann, U., Saenger, W., Mitsui, Y., Nakamura, K., Borisov, S., Tischenko, G., Kolyakov, P., & Pavlovsky, S. (1983) *Trends Biochem. Sci. 8*, 364–369.

Hoffman, E., & Rüterjans, H. (1988) *Eur. J. Biochem. 177*, 539–560.

Howard, A. J., Gilliland, G. L., Finzel, B., Poulos, T. L., Ohlendorf, D. H., & Saleeme, F. R. (1987) *J. Appl. Crystallogr. 20*, 383–387.

Iida, S., & Ooi, T. (1969) *Biochemistry 27*, 3242–3246.

Jones, T. A. (1987) *J. Appl. Crystallogr. 11*, 268–272.

Kiefhaber, T., Grunert, H.-P., Hahn, U., & Schmid, F. X. (1990a) *Biochemistry 29*, 6475–6480.

Kiefhaber, T., Schmid, F. X., Renner, M., Hinz, H.-J., Hahn, U., & Quaas, R. (1990b) *Biochemistry 29*, 8250–8257.

Koepke, J., Maslowska, M., Heinemann, U., & Saenger, W. (1989) *J. Mol. Biol. 206*, 475–488.

Kostrewa, D., Choe, H. W., Heinemann, U., & Saenger, W. (1989) *Biochemistry 28*, 7592–7600.

Lattman, E. E., & Love, W. E. (1972) *Acta Crystallogr. B 26*, 1854–1857.

Lenz, A., Cordes, F., Heinemann, U., & Saenger, W. (1991) *J. Biol. Chem. 266*, 7661–7667.

Luzzati, P. V. (1952) *Acta Crystallogr. 5*, 802–810.

MacKerell, A. D., Rigler, R., Nilsson, L., Hahn, U., & Saenger, W. (1987) *Biophys. Chem. 26*, 247–261.

MacKerell, A. D., Nilsson, L., Rigler, R., & Saenger, W. (1988) *Biochemistry 27*, 4547–4556.

MacKerell, A. D., Nilsson, L., Rigler, R., Heinemann, U., & Saenger, W. (1989) *Proteins 6*, 20–31.

MacKerell, A. D., Rigler, R., Hahn, U., & Saenger, W. (1991) *Biochim. Biophys. Acta 1073*, 357–365.

Malin, R., Zielenkiewicz, P., & Saenger, W. (1991) *J. Biol. Chem. 266*, 4848–4852.

Martin, P. D., Tulinsky, A., & Walz, F. G., Jr. (1980) *J. Mol. Biol. 136*, 95–97.

McNutt, M., Mullins, L. S., Raushel, F. M., & Pace, C. N. (1990) *Biochemistry 29*, 7572–7576.

Nishikawa, S., Moriako, H., Kim, H. J., Fuchimura, K., Tanaka, T., Uesugi, S., Hakoshima, T., Tomita, K., Ohtsuka, E., & Ikehara, M. (1987) *Biochemistry 26*, 8620–8624.

Osterman, H. L., & Walz, F. G., Jr. (1979) *Biochemistry 17*, 4124–4130.

Pace, C. N., & Creighton, T. E. (1986) *J. Mol. Biol. 188*, 477-486.
Pace, C. N., & Grimsley, G. R. (1988) *Biochemistry 27*, 3242-3246.
Phillips, S. (1980) *J. Mol. Biol. 142*, 531.
Ramachandran, G. N., & Sashisekharan, V. (1968) *Adv. Protein Chem. 23*, 283-437.
Ramakrishnan, C., & Ramachandran, G. N. (1965) *Biophys. J. 5*, 909-933.
Ravichandran, V., & Subramanian, E. (1981) *Int. J. Pept. Protein Res. 18*, 121-126.
Sato, S., & Egami, F. (1957) *J. Biochem. 44*, 753-757.
Schimada, I., & Inagaki, F., (1990) *Biochemistry 29*, 757-764.
Sevcik, J., Dodson, E. J., & Dodson, G. G. (1991) *Acta Crystallogr. B47*, 240-253.
Shirley, B. A., Stanssens, P., Steyaert, J., & Pace, C. N. (1989) *J. Biol. Chem. 264*, 11621-11625.
Steyaert, J., Hallenga, K., Wyns, L., & Stanssens, P. (1990) *Biochemistry 29*, 9064-9072.
Steyaert, J., Opsomer, C., Wyns, L., & Stanssens, P. (1991) *Biochemistry 30*, 494-499.
Sugio, S., Amisaki, T., Ohishi, H., & Tomita, K.-I. (1988) *J. Biochem. 103*, 354-366.
Takahashi, K. (1971) *J. Biochem. 70*, 945-960.
Takahashi, K. (1985) *J. Biochem. 98*, 815-817.
Takahashi, K., & Moore, S. (1982) *The Enzymes 15*, 435-468.
Walz, F. G., Jr., & Hooverman, L. (1973) *Biochemistry 15*, 2837-2842.
Walz, F. G., Jr. & Kitareewan, S. (1990) *J. Biol. Chem. 265*, 7127-7137.
Walz, F. G., Jr., Osterman, H. L., & Libertin, C. (1979) *Arch. Biochem. Biophys. 195*, 95-102.

Uniform ^{15}N Labeling of a Fungal Peptide: The Structure and Dynamics of an Alamethicin by ^{15}N and ^{1}H NMR Spectroscopy†

Adelinda A. Yee and Joe D. J. O'Neil*
Department of Chemistry, University of Manitoba, Winnipeg, Manitoba R3T 2N2, Canada
Received July 15, 1991; Revised Manuscript Received December 23, 1991

ABSTRACT: An alamethicin, secreted by the fungus *Trichoderma viride* and containing a glutamine at position 18 instead of the usual glutamic acid, has been uniformly labeled with ^{15}N and purified by HPLC. The extent of ^{15}N incorporation at individual backbone and side-chain sites was found to vary from 85% to 92%, as measured by spin-echo difference spectroscopy. The proton NMR spectrum of the peptide dissolved in methanol was assigned using correlation spectroscopies and nuclear Overhauser enhancements (NOE) measured in the rotating frame. The ^{15}N resonances were assigned by the 2D $^{1}H-^{15}N$ correlation via heteronuclear multiple-quantum coherence experiment. NOEs and $^{3}J_{NHC^{\alpha}H}$ coupling constants strongly suggest that, in methanol, from Aib-3 to Gly-11, the peptide adopts a predominantly helical conformation, in agreement with previous ^{1}H NMR studies [Esposito, G., Carver, J. A., Boyd, J., & Campbell, I. D. (1987) *Biochemistry 26*, 1043-1050; Banerjee, U., Tsui, F.-P., Balasubramanian, T. N., Marshall, G. R., & Chan, S I. (1983) *J. Mol. Biol. 165*, 757-775]. The conformation of the carboxyl terminus (12-20) is less well determined, partly because the amino acid composition reduces the number of NOEs and coupling constants which can be determined by ^{1}H NMR spectroscopy. The $^{3}J_{NHC^{\alpha}H}$ in the C-terminus suggest the possibility of conformational averaging at Leu-12, Val-15, and Gln-19, an interpretation which is supported by a recent molecular dynamics simulation of the peptide [Fraternalli, F. (1990) *Biopolymers 30*, 1083-1099]. The dynamics at each side-chain and backbone nitrogen were measured by the heteronuclear $^{15}N\{^{1}H\}$ NOE, but these measurements could not confirm a model in which the carboxyl terminus experiences greater conformational freedom than the amino terminus.

Alamethicins are a mixture of hydrophobic peptides secreted by the soil fungus *Trichoderma viride* (Meyer & Reusser, 1967). The peptides are assembled enzymatically by nonribosomal processes (Reusser, 1967; Rindfleisch & Kleinkauf, 1976), are rich in the amino acid α-aminoisobutyric acid (Aib, B),[1] and usually contain an amino alcohol such as phenylalaninol (O) (Balasubramanian et al., 1981). The so-called peptaibophols are known for their antibacterial activity (Balasubramanian et al., 1981; Jen et al., 1987) and their ability to uncouple oxidative phosphorylation in mitochondria (Mathew et al., 1981). In black lipid bilayers, they induce a conductance which increases exponentially with applied voltage (Eisenberg et al., 1973; Latore et al., 1981), a behavior also exhibited by the peptides melittin (Tosteson & Tosteson, 1982), gramicidin (Anderson, 1984), and pardaxin (Zagorski et al., 1991). On this basis, these peptides have been used as

†Supported by the Natural Sciences and Engineering Research Council of Canada and the University of Manitoba.

[1] Abbreviations: Aib, α-aminoisobutyric acid; ATCC, American type culture collection; B, α-aminoisobutyric acid; cw, continuous wave; DQF-COSY, two-dimensional double-quantum filtered correlation spectroscopy; DSS, disodium 2,2-dimethyl-2-silapentane-5-sulfonate; γ, magnetogyric ratio; H_E, syn substituent of a primary amide; H_Z, anti substituent of a primary amide; HMQC, two-dimensional heteronuclear multiple-quantum correlated spectroscopy; HPLC, high-performance liquid chromatography; J, scalar coupling constant; NMR, nuclear magnetic resonance; NOE, nuclear Overhauser effect; NOESY, two-dimensional nuclear Overhauser enhancement spectroscopy; O, phenylalaninol; ROESY, rotating frame nuclear Overhauser spectroscopy; TOCSY, total correlation spectroscopy; TPPI, time-proportional phase incrementation; τ_c, rotational correlation time; Pho, phenylalaninol.

0006-2960/92/0431-3135$03.00/0